Second Sound in Square and Cubical Cavities*

PHILIP J. BENDT
Los Alamos Scientific Laboratory, University of California, Los Alamos, New Mexico
(Received 28 May 1964)

The response of closed square and cubical cavities to linear standing waves of second sound in helium II has been studied. In a square cavity, when the number of half-wavelengths n along one side is even, a linear wave in the x direction couples loosely with the y direction, producing standing waves in both directions at two resonant frequencies, in a narrow doublet. The theory of the coupled waves is analogous to that for coupled LC electric circuits. When n is odd, a linear wave does not couple with the perpendicular directions. However, owing to quadratic terms in the thermohydrodynamic equations, a small-amplitude wave at twice the frequency of the standing wave is generated, and this wave is present along both the x and y axes. A theory of these phenomena is presented, along with frequency, amplitude, phase, and Q measurements. The results are similar in cubical cavities, but the number of available coupled-wave modes is reduced by cancellation of waves, due to the symmetry of the cavity.

I. INTRODUCTION

SECOND sound[1] in helium II is wave motion in which the normal fluid component and superfluid component oscillate out of phase, the total density of the liquid remaining very nearly constant. Since the entropy of the liquid resides in the excitations which comprise the normal fluid component, an increase in normal fluid density ρ_n corresponds to an increase in temperature T. T in second sound is therefore analogous to pressure in ordinary sound in a gas.

If quadratic terms and terms involving viscosity η are dropped from the thermohydrodynamic equations for helium II, and if pressure gradients and body forces are set equal to zero, the following differential equations obtain:

$$\partial^2 F/\partial t^2 = u^2 \nabla^2 F \tag{1a}$$

or

$$\partial^2 \mathbf{F}/\partial t^2 = u^2 \nabla (\nabla \cdot \mathbf{F}), \tag{1b}$$

where u is the velocity of second sound and F or $\mathbf{F}$ is any one of the variables T', S', ρ_n', ρ_s', $\mathbf{v}_n$, $\mathbf{v}_s$, $\mathbf{r}_n$, and $\mathbf{r}_s$. These are the fluctuating parts of the temperature T, entropy S, normal fluid density ρ_n, and superfluid density ρ_s; and the normal and superfluid velocities $\mathbf{v}$ and displacements $\mathbf{r}$. In a rectangular closed cavity with origin at one corner and sides of lengths a, b, and c in the x, y, and z directions, the standing wave solution of Eq. (1a) for T' is[2]

$$T' = \sum_n \sum_m \sum_p T'_{nmp} \exp(i\omega_{nmp} t) \times \cos\frac{n\pi}{a}x \cos\frac{m\pi}{b}y \cos\frac{p\pi}{c}z, \tag{2}$$

where T'_{nmp} are the amplitudes, and n, m, and p are integer numbers of half-wavelengths along the sides. The cosine functions are chosen to satisfy the boundary conditions at the walls; sine functions are used for the velocity waves. The frequencies ω_{nmp} are discrete and are given by

$$\omega_{nmp} = \pi u \left[\left(\frac{n}{a}\right)^2 + \left(\frac{m}{b}\right)^2 + \left(\frac{p}{c}\right)^2\right]^{1/2}. \tag{3}$$

We designate standing waves in one direction as linear modes, and waves involving two or three directions as compound modes. When a cavity is excited by a heater at a single frequency, the triple sum in Eq. (2) is reduced to a single term, except for degenerate modes.

We have found it informative to study linear standing wave resonances of second sound in closed rectangular cavities having two or three sides equal in length. Because of the terms omitted in deriving Eqs. (1a) and (1b), the solution above does not describe the observations. Before giving a more complete theory, we wish to state the differences between the experimental results and the predictions of the above simple theory, for a cavity with $a=b\neq c$.

(1) When n is even, a linear mode in the x direction will couple loosely with the y direction. We then have standing waves in both directions, at two resonant frequencies, separated by a small frequency difference $2\Delta\omega$. At $\omega_n+\Delta\omega$, the x and y waves are in phase, while at $\omega_n-\Delta\omega$, the phases differ by π. We wish to emphasize that these resonances do not constitute compound modes, for the x and y waves have different amplitudes, and the resonances occur at ω_n rather than $\sqrt{2}\omega_n$.

(2) When n is odd, a linear mode in the x direction of frequency ω_n does not couple with the y direction, and a single large resonance is observed. However, due to quadratic terms in the thermohydrodynamic equations, the wave of frequency ω_n is always accompanied by a small-amplitude wave of frequency $2\omega_n$. For this wave the number of half-wavelengths is even, and the $2\omega_n$ wave does couple with the y direction. At resonance, a small-amplitude wave of frequency $2\omega_n$ is observed in both the x and y directions, giving direct experimental evidence of the quadratic terms in the thermohydrodynamic equations.

The next four sections are devoted to a theory of resonances in square cavities. These are followed by a

* Work performed under the auspices of the U. S. Atomic Energy Commission.

[1] K. R. Atkins, *Liquid Helium* (Cambridge University Press, Cambridge, England, 1959), Chap. 5.

[2] J. W. Strutt (Baron Rayleigh), *Theory of Sound* (Dover Publications, Inc., New York, 1945), 2nd ed., Vol. II, p. 70.

description of our apparatus, and the experimental results for square cavities. The last section discusses the extension of the theory to cubical cavities, and the results for cubical cavities.

II. THERMOHYDRODYNAMIC EQUATIONS

London[3] gives the following equations for helium II, intended to be correct through quadratic terms:

$$\partial \mathbf{v}_s/\partial t+(\mathbf{v}_s\cdot\nabla)\mathbf{v}_s = -\nabla p/\rho+S\nabla T-\nabla\phi+\rho_n\nabla|\mathbf{v}_n-\mathbf{v}_s|^2/2\rho, \quad (4)$$

where p is the pressure, S is the entropy per g, ρ the total fluid density, and φ the potential function for the gravity force.

$$\partial \mathbf{v}_n/\partial t+(\mathbf{v}_n\cdot\nabla)\mathbf{v}_n = -\nabla p/\rho-\rho_s S\nabla T/\rho_n-\nabla\phi-\rho_s\nabla|\mathbf{v}_n-\mathbf{v}_s|^2/2\rho -\Gamma(\mathbf{v}_n-\mathbf{v}_s)/\rho_n-\eta\nabla\times\nabla\times\mathbf{v}_n/p_n +(2\eta+\eta')\nabla(\nabla\cdot\mathbf{v}_n)/\rho_n. \quad (5)$$

Γ is the conversion rate of superfluid to normal fluid, and η and η' are the first and second coefficients of viscosity. The continuity equations are $\partial\rho/\partial t+\nabla\cdot\rho\mathbf{v}=0$; $\partial\rho S/\partial t+\nabla\cdot\rho S\mathbf{v}_n=0$; $\partial\rho_n/\partial t+\nabla\cdot\rho_n\mathbf{v}_n=\Gamma$; and $\partial\rho_s/\partial t+\nabla\cdot\rho_s\mathbf{v}_s=-\Gamma$; where $\mathbf{v}$ is the velocity of the total fluid. If $\Gamma=0$ and the fluid is considered to be incompressible, then $\rho_n\mathbf{v}_n=-\rho_s\mathbf{v}_s$.

We use these equations in two ways. First, we derive a wave equation including attenuation by viscosity, but omitting the quadratic terms in Eqs. (4) and (5). Second, we calculate the amplitude of the wave of frequency $2\omega_n$ generated in the liquid by a driven wave of frequency ω_n. The wave equation for $\mathbf{v}_n$ including viscosity is

$$\frac{\partial^2\mathbf{v}_n}{\partial t^2}=u^2\nabla(\nabla\cdot\mathbf{v}_n)+\frac{\eta+\eta'}{\rho_n}\frac{\partial}{\partial t}\nabla(\nabla\cdot\mathbf{v}_n)+\frac{\eta}{\rho_n}\frac{\partial}{\partial t}\nabla^2\mathbf{v}_n. \quad (6)$$

The wave equation Eq. (1b) is seen to include only the first term on the right. The only solution of Eq. (6) which has frequency ω_n given by Eq. (3), with m and p equal to zero, is a plane wave. However, we know the tangential velocity of $\mathbf{v}_n$ along the walls at the sides of the plane wave is zero, due to viscosity. One way out of this dilemma is a hydrodynamic model in which the plane wave is separated from the side walls by a thin boundary layer, in which there are large temperature and velocity gradients.

The justification for assuming a distinct boundary layer is a large Reynolds number N_R, which we take to be $v_n\rho_n\lambda/4\eta$, where λ is the wavelength of second sound waves. We have used $\lambda/4$ for the characteristic length because it is the largest distance normal fluid can be displaced from equilibrium by a large amplitude wave. In the cavity, N_R is a function of x and t. Average values of N_R for our experiments, were of the order of 10^4.

[3] F. London, *Superfluids* (John Wiley & Sons, Inc., New York, 1954), Vol. II, pp. 130–132.

TABLE I. Liquid-helium analogs for a second sound wave of transmission line properties.

Transmission line property	Liquid-helium analog
Distance along line, x	Distance from heater, x
Voltage, $V(x)$	Temperature fluctuation, $T'(x)$
Current, $i(x)$	Heat current, $\rho ST\mathbf{v}_n(x)A$[a]
Capacitance per cm, C	Heat capacity per cm, ρAC_p[a]
Inductance per cm, L	$(\rho AC_pu^2)^{-1}$
Wave velocity, u	Sound velocity, u
Characteristic impedance $\mathbf{Z}_k$	$\approx(\rho AC_pu)^{-1}$[b]

[a] S is the entropy per g, C_p is the heat capacity per g, and A is the cross-sectional area of the cavity.
[b] $(\rho AC_pu)^{-1}$ neglects dissipative terms.

The thickness δ of the boundary layer is approximately equal to $C(\lambda\eta/4v_n\rho_n)^{1/2}$, where C is a numerical factor given by various authors as 3.4, 4.8, and 5.5.[4] Through the factor $\lambda^{1/2}$, δ is proportional to $\omega^{-1/2}$. In our experiments, with $\omega/2\pi=10^3$, δ was approximately 0.3 mm, which is less than 1% of the width of the cavity.

III. THE COUPLING CONSTANT K

Consider a driven linear standing wave in the x direction. The transfer of energy from this wave to a wave in the y direction is proportional to K^2, where K is the "coupling constant." K is zero unless the linear modes are degenerate, i.e., unless the cavity is square. Since energy is transferred to the y direction from both side walls $y=0$ and $y=a$, K is also zero if the number of half-wavelengths n is odd, for then the waves generated at the two side walls exactly cancel.

A cavity excited in a linear mode is analogous to an electric transmission line,[5] and we use transmission line theory to show how a linear mode is driven. Table I lists the liquid-helium analogs of transmission line properties. Experimentally, the wall of the cavity at $x=0$ is a heater, whose temperature varies as $e^{i\omega t}$.

When a driving emf $=\mathcal{E}_0e^{i\omega t}$ is applied at the end of an infinitely long transmission line, whose characteristic impedance is $\mathbf{Z}_k$, the current along the line is given by[6]

$$\mathbf{i}(x,t)=(\mathcal{E}_0/\mathbf{Z}_k)\exp[-i\omega(x/u-t)-\alpha x], \quad (7)$$

u is the wave velocity, α is an attenuation coefficient, and the vector quantities are complex numbers.

If we now terminate the line at $x=n\lambda/2$; if the reflection coefficients at both ends equal -1; if ω equals the resonant frequency ω_n; and if α is small, then

$$\mathbf{i}(x,t)=(\mathcal{E}_0/\mathbf{Z}_k)\exp(i\omega_nt-\alpha x) \times[Qe^{-i\pi/2}\sin(\omega_nx/u)+(1-x/a)e^{i\omega nx/u}], \quad (8)$$

where $Q=V_0/\mathcal{E}_0$ and V_0 is the amplitude of the voltage

[4] L. Prandtl and O. G. Tietjens, *Applied Hydro- and Aeromechanics* (Dover Publications, Inc., New York, 1957), p. 67; H. L. Dryden, F. D. Murnaghan, and H. Bateman, *Hydrodynamics* (Dover Publications, Inc., New York, 1956), p. 349; L. M. Milne-Thomson, *Theoretical Hydrodynamics* (The Macmillan Company, New York, 1955), 3rd ed., p. 569.
[5] See Ref. 1, pp. 141–142.
[6] L. Page and N. I. Adams, *Principles of Electricity* (D. Van Nostrand Company, Inc., New York, 1949), 2nd ed., pp. 533–544.

standing wave. The first term is the large resonating current, and the second term, equal at $x=0$ to the current going into an infinitely long line, supplies the energy dissipated by the resonating current. The power input $\mathbf{P}$ to both lines is the same,

$$\mathbf{P}=(\mathcal{E}_0^2/\mathbf{Z}_k)\exp(i2\omega_n t). \tag{9}$$

Equations (7), (8), and (9) also apply to linear second sound waves if the analogs in Table I are substituted. We rewrite Eq. (9) for an uncoupled second sound wave,

$$P_x'=ac\rho C_p u T_h^2\exp(i2\omega_n t), \tag{10}$$

where ac is the area of the heater and T_h is the amplitude of the temperature oscillations of the heater. The resulting second sound temperature standing wave is

$$T'(x,t)=T_x'\cos(\omega_n x/u)\exp(i\omega_n t), \tag{11}$$

where T_x' is the amplitude of the wave. The side walls at $y=0$ and $y=a$ are not heaters, and remain at the equilibrium temperature T_0. The wave in the y direction is driven by the temperature difference $-T'(x,t)$ across the boundary layers at $y=0$ and $y=a$ [the $\int_0^a T'^2(x,t)dx$ is a positive quantity]. The power input to the y wave is

$$P_y=ac\rho C_p u(KT_x')^2\exp(i2\omega_n t). \tag{12}$$

Equation (12) serves as a definition of K. The wave in the y direction transfers energy back into the x wave, giving, for the power input to the coupled x wave,

$$P_x=ac\rho C_p u[T_h^2+(KT_y')^2+2KT_hT_y'\cos\gamma]\exp(i2\omega_n t), \tag{13}$$

where γ is the phase angle between T_h and T_y'.

Setting $\gamma=0$, the Q's of the coupled linear modes are $Q_x=T_x'/(T_h+KT_y'-KT_x')$ and $Q_y=T_y'/(KT_x'-KT_y')$. If we assume $Q_x=Q_y=Q$, T_y' can be eliminated from these relations, giving

$$T_x'/T_h=Q(1+KQ)/(1+2KQ). \tag{14}$$

If K goes to zero, Eq. (14) reduces to $Q=T_x'/T_h$, which is the relation for an uncoupled x wave. Experimentally, we find KQ is apparently independent of frequency, and we set $KQ=N$. For our square cavity, $|N|\approx 5$, and in this instance, and for larger values of N, $T_x'/T_h\approx Q/2$.

IV. THE DOUBLE RESONANCES IN A SQUARE CAVITY

We write the wave equation Eq. (6) for plane waves in the x and y directions as follows:

$$\frac{\partial^2 v_x}{\partial t^2}-B\left(\frac{u}{\omega_n}\right)^2\frac{\partial}{\partial t}\frac{\partial^2 v_x}{\partial x^2}-u^2\frac{\partial^2 v_x}{\partial x^2}=0, \tag{15}$$

$$\frac{\partial^2 v_y}{\partial t^2}-B\left(\frac{u}{\omega_n}\right)^2\frac{\partial}{\partial t}\frac{\partial^2 v_y}{\partial y^2}-u^2\frac{\partial^2 v_y}{\partial y^2}=0, \tag{16}$$

where v_x and v_y are scalar normal fluid velocities, and $B=\omega_n^2(2\eta+\eta')/u^2\rho_n$. The solutions of Eqs. (15) and (16), which satisfy the boundary conditions, are $v_x=\sin(\omega_n x/u)\ F_x(t)$ and $v_y=\sin(\omega_n y/u)\ F_y(t)$. The equations for F_x and F_y are

$$d^2F_x/dt^2+BdF_x/dt+\omega_n^2F_x=0, \tag{17}$$

$$d^2F_y/dt^2+BdF_y/dt+\omega_n^2F_y=0. \tag{18}$$

We are interested in solutions F_x and F_y when the waves are coupled. We therefore add Kd^2F_y/dt^2 and Kd^2F_x/dt^2 to the right sides of Eqs. (17) and (18), respectively.[7] The coupled equations lead to the following equation for F_x:

$$(1-K^2)D^4F_x+2BD^3F_x+(B^2+2\omega_n^2)D^2F_x+2B\omega_n^2DF_x+\omega_n^4F_x=0, \tag{19}$$

where D stands for d/dt. We let $F_x=v_{x0}e^{i\omega t}e^{-\beta t}$, where v_{x0} is the amplitude of the wave at $t=0$. We drop all terms in β^2, βB, and B^2, as being second order. The equation for ω then is

$$(1-K^2)\omega^4-2\omega_n^2\omega^2+\omega_n^4=0. \tag{20}$$

This has two solutions, $\omega_1=\omega_n(1+K)^{-1/2}$ and $\omega_2=\omega_n(1-K)^{-1/2}$. The frequency difference is $\omega_2-\omega_1=2\Delta\omega\approx K\omega_n$. The frequencies ω_1 and ω_2 are the natural frequencies of the undriven, but coupled, perpendicular modes. They are also very nearly equal to the resonant frequencies when the x wave is driven. At frequencies near ω_n, the functions F_x and F_y are analogs of the currents in coupled resonant LC circuits. The exact resonant frequencies and phases, and the behavior of F_x and F_y near to and between the resonances, can be obtained from detailed analysis of coupled LC circuits.[8]

When n is odd, and the linear x wave is not coupled, $\beta=B/2$, and $Q=\omega_n/2\beta$. When the waves are coupled, β is obtained from Eq. (19), and is a function of ω:

$$\beta=(B/2)[1+K^2\omega^2/(\omega_n^2-\omega^2)]^{-1}. \tag{21}$$

For the uncoupled wave, $Q=\omega_n/\delta\omega$, where $\delta\omega$ is the width of the resonance at $\sqrt{2}/2$ of the maximum amplitude. Because of the frequency dependence of β, we have not applied this relation when the modes are coupled.

V. GENERATING THE DOUBLE-FREQUENCY WAVE

A linear standing second sound wave of frequency ω is always accompanied by a small-amplitude wave of frequency 2ω, generated in the liquid by the quadratic terms in the thermohydrodynamic equations, Eqs. (4) and (5). In Eqs. (4) and (5), we write T, S, ρ_n, and ρ_s as the sum of the equilibrium values (subscript zero) and the oscillating parts (superscript prime). Throughout the derivation, the order of a term equals the number of factors which are primed, multiplied by the number of factors $\mathbf{v}_n$ or $\mathbf{v}_s$. Third-order terms are dropped. We also drop from Eqs. (4) and (5) the terms

[7] We assume the K introduced here is defined by Eq. (12). The identity has not been proven in detail.

[8] See Ref. 6, pp. 499–517.

including ∇p, $\nabla\phi$, and Γ. Since we work at sufficiently low temperature so that $\rho_s \gg \rho_n$, we assume $\mathbf{v}_n \gg \mathbf{v}_s$. Equation (5) then reduces to

$$\partial \mathbf{v}_n/\partial t = -\rho_{s0}S_0\nabla T'/\rho_{n0} - \rho_{s0}S'\nabla T'/\rho_{n0} - \rho_s' S_0\nabla T'/\rho_{n0} - \nabla \mathbf{v}_n^2 - \rho_n'(\partial \mathbf{v}_n/\partial t)/\rho_{n0} - \eta\nabla\times\nabla\times\mathbf{v}_n/\rho_{n0} + 4\eta\nabla(\nabla\cdot\mathbf{v}_n)/3\rho_{n0}, \quad (22)$$

where, for simplicity, we have used the Stokes relation $\eta' = -2\eta/3$. We seek plane-wave solutions in the x direction. Using the thermodynamic relation for constant pressure $TdS = C_p dT$, and the continuity equation for ρS with ρ constant, we obtain

$$\frac{\partial T'}{\partial t} = -\frac{T_0}{C_p}\left[S_0\frac{\partial v_n}{\partial x} + S'\frac{\partial v_n}{\partial x} + v_n\frac{\partial S'}{\partial x}\right], \quad (23)$$

where v_n is the scalar value of $\mathbf{v}_n$.

Differentiating Eq. (22) with respect to time, substituting Eq. (23), using the continuity equations, and making several approximations, we obtain

$$\frac{\partial^2 v_n}{\partial t^2} = u^2\frac{\partial^2 v_n}{\partial x^2} - 3u^2\frac{\partial v_n}{\partial x}\int\frac{\partial^2 v_n}{\partial x^2}dt - 2u^2\frac{\partial^2 v_n}{\partial x^2}\int\frac{\partial v_n}{\partial x}dt - u^2 v_n\int\frac{\partial^3 v_n}{\partial x^3}dt - \frac{\partial^2 v_n^2}{\partial x\partial t} + \frac{\partial v_n}{\partial x}\frac{\partial v_n}{\partial t} + \frac{4\eta}{3\rho_{n0}}\frac{\partial}{\partial t}\left(\frac{\partial^2 v_n}{\partial x^2}\right), \quad (24)$$

where $u^2 = (\rho_s/\rho_n)S_0^2 T_0/C_p$, and we have dropped a term of order $\rho_n/\rho_s \ll 1$. We now substitute

$$v_n = F_\omega(t)\sin\omega x/u + F_{2\omega}(t)\sin 2\omega x/u \quad (25)$$

for the linear terms in Eq. (24), and $v_n = F_\omega(t)\sin\omega x/u$ for the quadratic terms. This approximation artificially eliminates waves of higher frequency than 2ω. We have removed the space dependence from Eq. (24), which now yields two equations,

$$d^2F_\omega/dt^2 + (4\eta\omega^2/3\rho_{n0}u^2)dF_\omega/dt + \omega^2 F_\omega = 0, \quad (26)$$

and

$$d^2F_{2\omega}/dt^2 + (16\eta\omega^2/3\rho_{n0}u^2)dF_{2\omega}/dt + 4\omega^2 F_{2\omega} - (3\omega^3/u)F_\omega\int F_\omega dt - (\omega/2u)F_\omega dF_\omega/dt + (\omega/u)dF_\omega^2/dt = 0. \quad (27)$$

If we add to the right side of Eq. (26) a driving term, representing the power supplied by the heater, we can set $F_\omega = v_\omega \exp i\omega t$ and $F_{2\omega} = v_{2\omega}\exp i2\omega t$, where v_ω and $v_{2\omega}$ are the steady-state amplitudes of the driven wave and the double-frequency wave, respectively. From Eq. (26) we obtain an expression for the Q of the cavity, for an uncoupled x wave,

$$Q = (3\rho_{n0}u^2/4\eta\omega_n). \quad (28)$$

From Eq. (27) we obtain a relation between $v_{2\omega}$ and v_ω,

$$v_{2\omega} = v_\omega^2(9Q/16u). \quad (29)$$

In a second sound wave, v_n is related to T' by $v_n = \rho_{s0}S_0T'/\rho_{n0}u$.[5] Making this substitution, we find the amplitudes of the temperature waves are related by

$$T'_{2\omega} = (T_\omega')^2(9\rho_{s0}S_0Q/16\rho_{n0}u^2). \quad (30)$$

Anticipating the experimental results, Eq. (30) was found to be approximately correct if experimental values of Q are used. However, the experimental Q's are about 10^{-4} as large as calculated from Eq. (28). From this we conclude that normal fluid viscosity is not the major source of dissipation in a second sound cavity. A larger source of dissipation may be exchange of thermal energy with the walls, which are not perfect insulators, or may be mutual friction between the normal and superfluid components.

VI. EXPERIMENTAL APPARATUS

The square second sound cavity that we used was 3.99 cm on a side, and 2.38 cm high (inside dimensions). The distances between walls in the x and y directions differed by not more than 0.005 cm, corresponding to a difference in resonant frequencies of 1.25 cps at 10^3 cps. The four walls at $x=0$, $x=a$, $y=0$, and $y=a$ were 500-Ω/sq carbon resistance strips, with 1-mm-wide conducting strips painted along the top and bottom edges. The top and bottom of the cavity were closed with flat micarta surfaces. The cubical cavities we used were of similar construction, and their dimensions are given in Sec. IX.

The $x=0$ wall of the cavity was the heater and was connected by miniature coaxial cable to an audio sine-wave oscillator, which supplied 10 to 40 V, peak-to-peak. Three other walls of the cavity served as detectors of temperature oscillations, through their thermal coefficient of electrical resistance. The detector of the x wave in the square cavity had a resistance of 470 Ω at 1.47°K, and a temperature coefficient of −63 Ω/°K. It will be noted that the heater generated temperature oscillations, at double the frequency of the audio oscillator, uniformly and in phase over an entire wall. Therefore, cavity modes which require the temperature oscillations to vary across the heater wall were not generated.

During measurements, the cavity was completely submerged in a bath of helium II. Helium in the cavity communicated with the bath through 2-mm-diam holes provided at the corners. The temperature was determined from the vapor pressure of the bath, measured with an oil manometer. The high thermal conductivity of superfluid helium assured that the temperature inside the cavity was close to that of the bath. Measurements were made between 1.45 and 1.5°K.

The signal from the audio oscillator also went to a frequency counter and a frequency doubling circuit. The latter was used to drive the horizontal sweep of an oscilloscope while phase measurements were made, using Lissajous patterns. An electrical drive was

TABLE II. Square cavity resonances.

Number of wavelengths along a side	x-wave resonant frequencies at 1.48°K (cps)	x-wave doublet separation $2\Delta\omega$ (cps)	Width at 0.71 maximum amplitude (cps)	Frequency width for phase change $3\pi/4$ to $5\pi/4$ (cps)	Cavity Q, calculated from $Q=\omega_n/\delta\omega$[a]	x-wave detector thermal amplitude for $V_h=20$ V (°K)
1/2	262.4		4.0	5.6	66	1.6×10^{-3}
1	499.6 512.4	12.8				1.6
3/2	754.0		4.0	3.4	189	1.3
2	987.4 1003.2	15.8				0.7
5/2	1262.8		3.2	3.6	395	0.6
3	1490.6 1507.2	16.4				3.8 1.0
7/2	1756.2		1.0	1.2	1756	4.4
4	1985.0 1998.2	13.2				2.2 1.3
9/2	2246.6		1.2	1.2	1872	4.1
5	2473.0 2490.0	17.0				2.9
Average		15.0	2.7	3.0		
Reduced average[b]	250.5					

[a] $\delta\omega$ is the width at 0.71 maximum amplitude.
[b] Each frequency is divided by the number of half-wavelengths before averaging. The frequency for ½-wavelength is omitted from the reduced average.

connected to the oscillator frequency control, so that frequencies could be swept at slow speeds, in order to plot the shape of resonances.

The resistance-strip detectors were biased with 0.5 mA dc, and the ac signals from them were amplified 10^4 times. The amplified signals at resonance were of the order of 1 V, while noise and pickup were 0.05 V or less. Signals from the x and y detectors were displayed simultaneously on a dual trace oscilloscope, and were also rectified, and plotted by a two-pen chart recorder.

VII. RESONANT FREQUENCIES AND AMPLITUDES

The frequencies and widths of the square cavity resonances are tabulated in Table II. When the number of half-wavelengths n is even, the resonances are doublets, on both the x and y detectors. Since the height of the cavity in the z direction was incommensurate with the (equal) sides in the x and y directions, waves in the z direction were not excited at the frequencies in Table II. If each single-resonance frequency, or doublet midpoint, is divided by n, the quotients are the same within experimental error, except for $n=1$, which is 4.7% high. We believe this indicates a small phase shift occurs at the reflecting walls of the cavity. Using the average of the above quotients (omitting $n=1$) to calculate the velocity of second sound gives 20.0 m/sec at 1.48°K, in good agreement with other measurements.[9]

The Q of the cavity is given by the resonant frequency ω_n divided by the difference of the frequencies corresponding to $\sqrt{2}/2$ of the maximum amplitude. The theory of resonant systems also tells us that the phase of an oscillating system, relative to the driving force, should change by $\pi/2$ between those two frequencies. We have used both amplitude and phase change to determine the width of the resonances when n is odd. The reason for the marked reduction in $\delta\omega$ for 7/2 and 9/2 wavelengths is not known.

The widths of the doublets $2\Delta\omega$ show no trend with frequency. From the relations $N=KQ$, $2\Delta\omega=K\omega_n$, and $Q=\omega_n/\delta\omega$, we obtain $2\Delta\omega=N\delta\omega$. From the average values given in Table II, we see $N\approx5$ in the square cavity.

It was found that when the heater covered an entire wall, it would not generate compound modes in the square cavity. In a separate experiment, the width of the heater was reduced to 1 cm, located at the center of the wall $x=0$. In addition to the frequencies listed in Table II, the cavity then resonated at 1420 cps, which is $\sqrt{2}$ times the frequency for two wavelengths along a side. This is the compound mode with $n=m=4$, and $p=0$, in Eq. (3).

The amplitudes of the resonances are proportional to the square of the peak-to-peak voltage V_h applied to the heater. This can be seen from the relation $dT/dt=(dq/dt)C_h^{-1}$, where dq/dt is the rate of heat input, and C_h is a heat capacity. $dq/dt=(V_h^2/4R)\exp(i\omega t)$, where R is the resistance of the heater, and the oscillator frequency is $\omega/2$. Integrating with respect to t, we obtain for the amplitude of the temperature wave

$$T_\omega'=V_h^2Q/4\omega RC_h. \tag{31}$$

[9] J. R. Pellam, Phys. Rev. **75**, 1183 (1949); R. D. Mauer and M. A. Herlin, *ibid.* **76**, 948 (1949).

TABLE III. Proportionality of T_ω' to V_h^2, and of $T_{2\omega}'$ to $T_\omega'^2$, for $n=3$. $T_{2\omega}'$ is the amplitude of the coupled wave. The temperature was 1.45°K.

Heater (volts) V_h	V_h^2	x-wave detector (volts×10^{-4}) (T_ω')	$T_\omega'\times10^7$ / V_h^2	$T_\omega'^2$	y-wave detector (volts×10^{-4}) $(T_{2\omega}')$	$T_{2\omega}'\times10^{-3}$ / $T_\omega'^2$
4	16	0.036	2.25			
6	36	0.080	2.22			
8	64	0.14	2.19			
10	100	0.22	2.20			
12.5	156	0.36	2.31			
15	225	0.55	2.44	0.303	0.029	0.96
20	400	0.95	2.38	0.903	0.085	0.94
25	625	1.30	2.08	1.69	0.170	1.01
30	900	1.89	2.10	3.57	0.320	0.90
Average values[a]			2.28			0.95

[a] T_ω' for $V_h=25$ and 30 V have been omitted from the average.

The variation in measured values of $2T_\omega'$ for $V_h=20$ V is given in Table II, where some numbers are large because Q is unexpectedly large. The detector voltage has been converted to peak-to-peak amplitude of temperature oscillation in Table II.

The proportionality of T_ω' to V_h^2, and of $T_{2\omega}'$ to $T_\omega'^2$ given by Eq. (30), is shown for $n=3$ in Table III. $T_{2\omega}'$ is the amplitude of the coupled y wave, as it is difficult to measure the amplitudes separately in the x wave. The deviations of the numbers in the fourth and seventh columns of Table III from the average values are probably experimental error, except that when V_h is larger than 20 V, T_ω' falls below the values predicted by the above relations, due to the increase in attenuation at large amplitudes.[10] The x and y waveforms for $n=3$ and $V_h=30$ V are shown in Fig. 1.

VIII. THE SQUARE CAVITY RESONANCES

The phase of the temperature oscillations of the x-wave detector relative to the voltage applied to the heater was measured for $\lambda/2=a$ at positions 1, 2, and 3, shown in Fig. 2. The phase increased with frequency from $3\pi/4$ at position 1, to π at maximum amplitude,

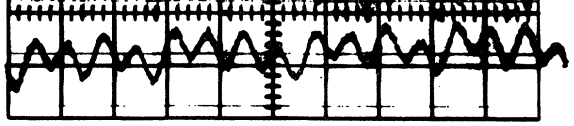

FIG. 1. Oscilloscope traces of the x wave (above) and y wave (below) in the square cavity when $3\lambda/2=a$. The x wave shows T_ω' (at 754 cps) with $T_{2\omega}'$ superimposed. The y wave shows only $T_{2\omega}'$. The oscilloscope sweep speed was 1 msec per large division and the sensitivity was 1 V per large division for the x wave, and 0.5 V per large division for the y wave. The heater voltage was 30 V.

[10] K. R. Atkins and K. H. Hart, Can. J. Phys. 32, 381 (1954).

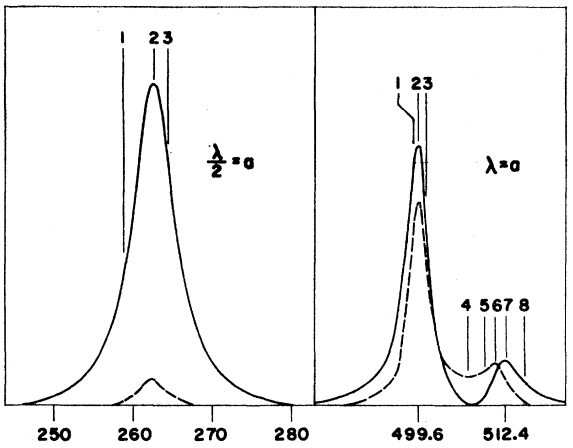

FIG. 2. Resonances in the square cavity, with sides of length a. The frequency increases to the right, and the numbers underneath are cps. Numbers above the resonances identify frequencies at which the phases were measured. The solid line is the x wave, and the dashed line is the y-wave. At $\lambda/2=a$, the y wave is at double the frequency of the x wave. The heater voltage was 15 V.

to $5\pi/4$ at position 3. The reason for the asymmetry of positions 1 and 2 with respect to the maximum amplitude is not known. Since the number of half-wavelengths is odd, it is clear that the temperature oscillation at the wall $x=a$ should be π out of phase with the heater.

When n is even, the resonances are doublets, as shown in Figs. 2 and 3. The y wave now couples with the frequency ω_n, and the $2\omega_n$ wave was not observed at low input voltages. The relative amplitudes of the peaks in the doublets have not been interpreted, and are seen to differ for different values of n. The phases of both the x and y waves, relative to the voltage applied to the heater, were measured for $\lambda=a$, at the positions indicated in Fig. 2, and are given in Table IV. The following observations are made about the double resonances and the phases:

(1) The frequency separation of the y-wave doublet is less than the separation of the x-wave doublet.

(2) The x-wave amplitude goes to zero between resonances, while the y-wave amplitude does not.

TABLE IV. Phases of the x- and y-wave detectors, relative to the heater voltage, for the double resonances in the square cavity, when $\lambda=a$.

Position in Fig. 2	x-wave phase	y-wave phase
1	0	π
2	$\pi/4$	$5\pi/4$
3	$\pi/2$	$3\pi/2$
4	$\pi/2$ (Zero amplitude)	$7\pi/4$
5	$7\pi/4$	~0
6	0	0
7	$\pi/4$	~0
8	$\pi/2$	$\pi/2$ (Zero amplitude)

TABLE V. Cubical cavity resonances.

Number of wavelengths along a side (linear modes)	Driven mode half-wave numbers[a]			x-wave resonant frequencies at 1.45°K (cps)	Reduced frequency[b] (cps)	Cavity Q, calculated from $Q=\omega_n/\delta\omega$			Detector phase at maximum amplitude[c]		
	n	m	p			x	y	z	x	y	z
1/2	1	0	0	246.0	246.0	60			π		
1	2	0	0	487.4	243.7	195	283	108	0	π	π
	2	1	0	540.0	241.5	148			π		
	2	2	0	683.8	241.8	204			0	π	π
3/2	3	0	0	725.8	241.9	161			π		
2	4	0	0	970.2	242.6	200	138	167	0	π	π
	4	2	0	1100.2	246.0	178			0		
5/2	5	0	0	1216.8	243.4	174			π		
	5	2	0	1313.6	243.9	155			π		
3	6	0	0	1461.6	243.6	209			0	π	π
	6	2	0	1535.8	242.9	154			0		
7/2	7	0	0	1700.8	243.0	243			π		
	6	4	0	1765.0	244.7	176			π		
4	8	0	0	1944.4	243.1	272			0	π	π
	8	2	0	2002.0	242.8	280			0		

[a] Coupled waves are omitted. n, m, and p are the number of half-wavelengths along the x, y, and z axes. Numbers for m and p are interchangeable, since y and z are symmetrical in the cavity.
[b] Resonant frequency divided by $(n^2+m^2+p^2)^{1/2}$.
[c] Phase is relative to voltage on heater, at $x=0$. The x-wave phase is taken at $x=a$.

(3) For the x wave, the phases for positions 6, 7, and 8 repeat the phases for positions 1, 2, and 3.

(4) Between positions 1 and 6, the x-wave phase increases by 2π, while the y-wave phase increases by π.

(5) At the low-frequency maximum, the x and y waves are π out of phase, while at the high-frequency y-wave maximum, they are in phase.

All five observations listed above would apply to a graph of the currents in coupled LC circuits, if one circuit only were driven by a generator whose frequency was swept through the (double) resonance. This verifies that the frequency-dependent parts of the solution of the coupled wave equations, discussed in Sec. IV, are the analogs of the currents in coupled LC circuits, at frequencies close to resonance.[8]

From the observed phase relations, we have deduced the temperature modes of oscillation at resonance in the square cavity. These are given in Fig. 4 for $\lambda=a$ and $2\lambda=a$; the extension to high frequencies is obvious.

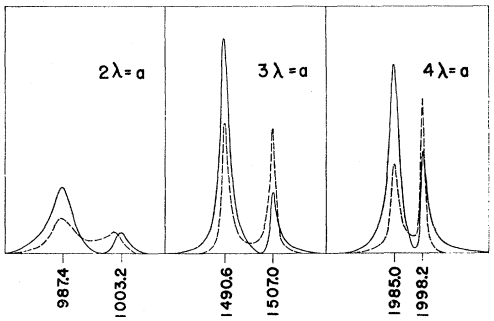

FIG. 3. Resonances in the square cavity, with sides of length a, when n is even. The frequency increases to the right, and the numbers underneath are cps. The solid line is the x wave, and the dashed line is the y wave. The heater voltage was 15 V.

These are not compound modes, but rather the superposition of two linear modes which may have different amplitudes. The heater is in contact only with the plane wave that it generates, and is separated by a boundary layer from the coupled wave. The nodal lines shown in Fig. 4 are therefore not in contact with the heater. Mode 2 is identical with the compound modes for $n=m$ and $p=0$. The compound modes, however, have the same amplitude of oscillation on all four walls, and the nodal lines do touch the walls, requiring that T_h' of the heater be zero at these points. The configuration shown in the lower right-hand corner of Fig. 4 was

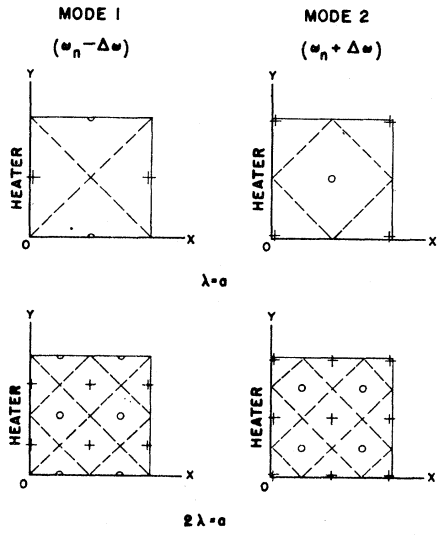

FIG. 4. Coupled-wave modes of the square cavity, when n is even. Dashed lines are the temperature nodal lines for the superimposed linear standing waves. + and 0 indicate positions of high- and low-temperature antinodes at a given time; one-half cycle later these are interchanged.

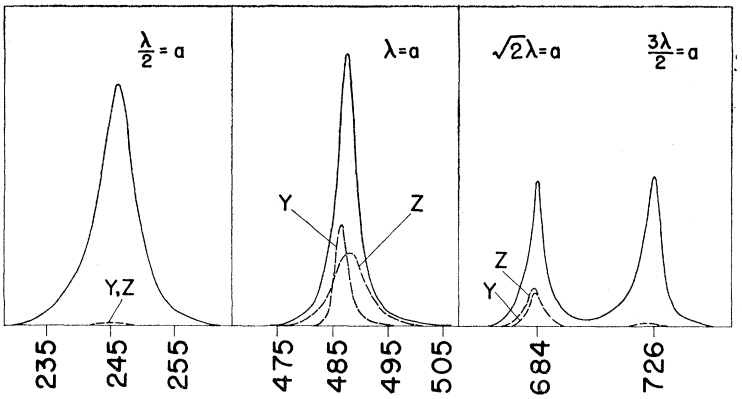

FIG. 5. Resonances in the cubical cavity, with edges of length a. The frequency increases to the right, and the numbers underneath are in cps. The solid line is the x wave. Mode B and mode C are superimposed when $\lambda=a$. The resonance for $\sqrt{2}\lambda=a$ is a compound mode. The heater voltage was 15 V.

generated as a compound mode with a narrow heater at the midpoint of the wall at $x=0$, as mentioned in Sec. VII.

IX. THE CUBICAL CAVITY RESONANCES

The first cubical cavity we used was 4 cm along each edge, and had resistance strip covering each wall, except for a 0.5-mm gap between walls. With this cavity, we did not observe any compound resonances. The results reported below were obtained with a second cubical cavity, 4.10 cm along each edge. The resistance strips were 3 cm square, centered in each wall, and mounted flush with the 0.55-cm micarta border which completed each wall. The distances between walls in the x, y, and z directions differed by not more than 0.003 cm, and the wall $x=0$ was the heater. The resonances are given in Table V, and include a number of compound modes.

When n was an odd integer, and $m=p=0$, the x wave did not couple with either the y or z directions. We observed single resonances, similar to those for $\lambda/2=a$ and $3\lambda/2=a$, shown in Fig. 5. The response of the y and z detectors was too weak to determine the frequency. The phase change of the x wave going through resonance was similar to that for the corresponding wave in the square cavity, and the phase at maximum amplitude equalled π at the wall $x=a$.

Symmetry conditions are important in determining the resonances of the cubical cavity when n is an even integer, and $m=p=0$. There are three coupling constants K_{xy}, K_{yz}, and K_{zx}, which can equal either $|K|$ or $-|K|$. Of the eight possible combinations of K's, the coupled modes resulting from six combinations cancel each other identically, due to symmetry. We are left with the two combinations in which all three K's have the same sign. These combinations are satisfied by only three coupled-wave modes. Using + to mean in phase with the heater, − to mean π out of phase, and 0 to mean zero amplitude, these modes are: +, +, +(mode A); +, 0, −(mode B); and +, −, 0(mode C). The symbols are in x, y, and z order. Modes B and C are coupled waves in two directions only, and are identical to mode 1 in Fig. 4. Modes B and C are alternate modes, not coupled to each other, and not separated by a frequency splitting.

Mode A for $n=2$ is shown in an isometric drawing in

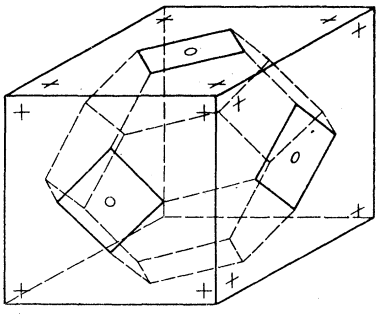

FIG. 6. Isometric drawing of the coupled-wave mode A in the cubical cavity when $n=2$. The intersection of the nodal surface with each wall forms a square, which has a diagonal length equal to $\lambda/2$. + and 0 indicate positions on the walls of high- and low-temperature antinodes at a given time; one-half cycle later these are interchanged.

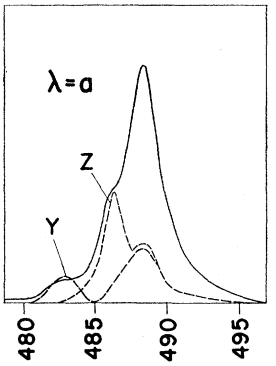

FIG. 7. Resonances in the modified cubical cavity, with edges approximately equal to a. The frequency increases to the right, and numbers underneath are in cps. The solid line is the x wave. The distance between walls in the y direction is 1% larger than in the x direction, and the distance in the z direction is 0.3% larger than in the x direction. Mode B and mode C each resonated twice, at the frequency for the x direction, and also at the frequency for the y, or z direction. The heater voltage was 15 V.

Fig. 6. The nodal surface consists of eight hexagons, arranged symmetrically in the corners of the cube. The intersection of the nodal surface with each wall of the cavity forms a square, turned 45° with respect to the edges, and having a diagonal length equal to $\lambda/2$. T' changes sign when the nodal surface is crossed. In this mode, the temperature oscillation adjacent to the heater wall, for 1/8 of the area, is π out of phase with the temperature oscillation adjacent to the remainder of the heater. For $n=4, 6, 8, \cdots$, the temperature distributions opposite the heater are also divided into areas having opposite signs, and therefore mode A was not excited with either heater configuration we used.

We observed modes B and C superimposed. They peaked at very nearly the same frequency, as seen for $\lambda=a$ in Fig. 5 (the difference in frequency is due to unequal cavity dimensions). The phase relations at maximum amplitude are given in Table V. We also show in Fig. 5 an apparent doublet, actually composed of single resonances at $\sqrt{2}\lambda=a$ ($n=m=2$; $p=0$) and $3\lambda/2=a$.

In a separate experiment, we decided to see if modes B and C could be separated by increasing the distance between walls in the y direction by 1%. While assembling the cavity, we inadvertently also increased the distance in the z direction by 0.3%. The resulting resonances for $\lambda=a$ are shown in Fig. 7. Each mode resonated twice, at the frequency for the x direction, and also at the frequency for the y or z direction. Unlike the doublets in the square cavity, the phase relations are the same at each resonant frequency in Fig. 7 (they are as listed in Table V).

PHYSICAL REVIEW VOLUME 136, NUMBER 4A 16 NOVEMBER 1964

Magnetic-Field Penetration and Breakdown of Surface Superconductivity I*

MYRON STRONGIN, DONALD G. SCHWEITZER, ARTHUR PASKIN, AND PAUL P. CRAIG
Brookhaven National Laboratory, Upton, New York
(Received 15 June 1964; revised manuscript received 31 July 1964)

Low-frequency low-field ac susceptibility measurements on type II and certain type I superconductors have shown complete diamagnetism, until the transition at some surface upper critical field H_{c3}. In this paper we describe measurements in a swept dc field which show that at sufficiently large sweep rates the ac field can be made to penetrate the superconductor, and the real part of the ac susceptibility will be dM/dH along the magnetization curve, with no observable transition at H_{c3}. At intermediate sweep rates, the value of the susceptibility becomes more diamagnetic and a partial transition is observed at H_{c3}. For the slowest sweeps and highest frequencies, essentially the full diamagnetic-susceptibility characteristic of the point-by-point measurements is obtained, along with a transition at H_{c3}. These results are of particular significance since they indicate that an ac field of small amplitude can be made to penetrate a type II superconductor in the mixed state, and can therefore be used to investigate the bulk properties. Two models which we have considered to explain our results are briefly discussed.

INTRODUCTION

IN this paper we report low-frequency low-field ac susceptibility measurements which have been made in "swept dc fields." In a previous paper[1] it was shown that in fixed dc fields the ac susceptibility showed complete sample diamagnetism (i.e., $-\frac{1}{4}\pi$) until the upper critical field H_{c3}.[2] In contrast to the measurements in fixed dc fields, the susceptibility measurements in swept dc fields can yield dM/dH of the magnetization curve up to H_{c2} and then the normal metal susceptibility above H_{c2}. These results are of particular significance since they indicate that the small ac field has penetrated the superconductor in the mixed state, and can thus be used to investigate the bulk properties of type II superconductors. The detailed results, which depend on the sweep rate, ac amplitude, and the ac frequency, are discussed.

RESULTS

Magnetization and ac measurements were made on a series of cylindrical alloy samples[1] subjected to various surface treatments. Both the ac and dc fields were parallel to the axes of the samples.

Sensitive ac susceptibility measurements were made in which the external dc field was increased and decreased at constant rates. Both the real component of the ac susceptibility (χ'), and the imaginary component (χ''), were studied as functions of dc sweep speeds.[3] By a proper choice of ac frequency, ac amplitude and dc sweep rate, χ' can be made less than completely diamagnetic in the region below H_{c3} and above the region of bulk diamagnetism, thereby indicating penetration of the ac field into the bulk of the

* This work was performed under the auspices of the U. S. Atomic Energy Commission.

[1] M. Strongin, A. Paskin, D. G. Schweitzer, O. F. Kammerer, and P. P. Craig, Phys. Rev. Letters 10, 442 (1964).

[2] Saint-James and P. G. de Gennes, Phys. Letters 7, 306 (1963).

[3] Under conditions of changing dc fields we define χ' and χ'' to be proportional to the real and imaginary parts of the mutual-inductance-bridge imbalance voltage.